Pergamon

Electrochimica Acta, Vol. 41, No. 14, pp. 2267–2273, 1996

0013-4686/96 $15.00 + 0.00

PII:S0013-4686(96)00054-0

A SEMIEMPIRICAL QUANTUM CHEMISTRY APPROACH TO POSSIBLE STRUCTURES AND ENERGIES OF HYDROGEN ATOMS ADSORBED ON Pt(100) AND Pt(111) CLUSTERS AT A SIMULATED Pt/AQUEOUS ELECTROCHEMICAL INTERFACE

C. F. ZINOLA and A. J. ARVIA*

Instituto de Investigaciones Fisicoquímicas Teóricas y Aplicadas (INIFTA), Universidad Nacional de La Plata, Sucursal 4, Casilla de Correo 16, (1900) La Plata, Argentina

(*Received* 10 *May* 1995; *in revised form* 29 *June* 1995)

Abstract—Extended Hueckel molecular orbital calculations for the adsorption of H-atoms in a simulated aqueous electrochemical environment on Pt(111) and Pt(100) clusters were made. Different adsorbate configurations were considered. H-atom adsorption on hollow sites coadsorbed with an on top OH-species for Pt(111), and H-atom adsorption on bridge sites for Pt(100) are favoured. At potentials lower than the hydrogen electrode equilibrium potential, H-adatom configurations involving subsurface Pt atoms can also be formed. For both Pt(111) and Pt(100), these structures are probably related to species involved in the H-atom electrosorption and hydrogen evolution reaction. Copyright © 1996 Elsevier Science Ltd

Key words: hydrogen, platinum, semiempirical methods.

1. INTRODUCTION

The Pt–H atom interaction plays a key role in electrochemistry, particularly at the Pt/aqueous solution interface in the range of potentials related to the H-adatom electrosorption equilibria, and hydrogen evolution reaction. Relevant data on these processes have been obtained on Pt single crystals involving both low and high Miller indices[1–7]. In principle, the formation and characteristics of H-adsorbates on Pt in a particular environment depend on the H-atom adsorption energy at the different adsorption sites[7–9]. It should be noted that in recent years Pt–H and Pt–H_2O interactions under ultra-high vacuum conditions, at well-defined single crystal surfaces, have been extensively studied[10–14], and the results obtained for those systems have encouraged us to attempt a quantum mechanics modelling of the Pt–H system at the Pt/aqueous electrochemical interface. In general, two main types of H-adatoms on Pt in an aqueous environment are distinguished in the range of potentials where the H-atom electrosorption takes place, namely, strongly and weakly bound H-adatoms dominating at Pt surfaces with a lower and a higher atom density, respectively. However, the real situation is more complex[15–18] as, for instance, the third anodic voltammetric peak related to H-adatom electrodesorption on Pt has been assigned to subsurface hydrogen adsorption[19]. Furthermore, a.c. impedance data[20, 21] have revealed that other H-adatom species would appear as intermediates in the course of the hydrogen evolution reaction on Pt in acid. This conclusion appears to be supported by data derived from electrochemically modulated infrared spectroscopy[22–24] and visible-infrared sum frequency generation techniques[25]. The formation of intermediates in the hydrogen evolution reaction has also been inferred from the analysis of potential relaxation curves[8, 9].

The situation outlined above suggested the convenience of attempting a quantum chemistry approach to surface species likely formed at a simulated Pt/aqueous electrochemical interface in order to discriminate the structure and energy of possible H-adsorbates. This is a relevant issue in dealing with, for instance, the interpretation of the complex electrosorption spectra of H-atoms on Pt in aqueous solution, and to provide a more realistic approach to the nature of H-atom intermediates involved in the hydrogen evolution reaction.

The possible structures and energies of H-adatoms were calculated on Pt(100) and Pt(111) clusters at a simulated Pt/aqueous electrochemical interface using the Extended Hueckel Molecular Orbital (EHMO) semiempirical procedure developed by Hoffmann[26, 27] and recently improved by Calzafferi[28–31]. This calculation procedure proved to be sufficiently simple and reliable to deal with the subject matter of this paper. In fact, the selection of the calculation procedure was determined by computational limitations and the size of the finite clusters involving transition metal atoms of a high atomic number.

2. THE CALCULATION PROCEDURE

The EHMO method was applied to describe the structural and electronic properties of the Pt–H

* Author to whom correspondence should be addressed.

system for a given geometry. The EHMO method is one of the simplest semiempirical methods available to describe the valence electronic structure, binding energies and chemical properties of large transition metal clusters involved in adsorption systems. It is worth noting that the EHMO method gives an overestimation and an underestimation in bonding forces, but the relative bonding structural stability is well described[28].

The EHMO method including a sum of two body electrostatic terms[27, 30, 31] makes possible the optimization of the adsorbate structure for a given geometry. Accordingly, ET, the gobal energy of the system, is calculated from the contribution of three terms, *ie*

$$\mathrm{ET} = E_{\mathrm{EHMO}} - \sum_{\mu} b_{\mu}^{0} E_{\mu}^{0} + \mathrm{RE} \tag{1}$$

where E_{EHMO} is the non-corrected EHMO total energy including monoelectronic terms; b_{μ}^{0} is the occupation number, E_{μ}^{0} is the valence state ionization potential (VSIP) of the μth atomic orbital, and RE is the repulsion energy correction term. RE is evaluated from E_{AB}, the contribution of the electrostatic repulsion energy between atoms A and B, separated from each other by the distance R_{AB}. Then,

$$\mathrm{RE} = \sum_{\mathrm{A}} \sum_{\mathrm{B}<\mathrm{A}} E_{\mathrm{AB}} \tag{2}$$

The EHMO method does not explicitly consider a term for the short-time repulsion energy between different atoms. To calculate the minimum adsorption energy and equilibrium distance between interacting atoms, the method was reformulated[29–31] by including firstly E_{AB}, a repulsion energy term, and secondly, $H_{\mu\nu}$, a distance-dependent exponential factor in the off-diagonal EHMO matrix elements. The former represents the difference between the coulombic interaction energy and the arithmetic mean of attractive interaction energy for A–B and B–A. Then,

$$E_{\mathrm{AB}} = \frac{Z_{\mathrm{A}} Z_{\mathrm{B}}}{R_{\mathrm{AB}}} - \frac{1}{2}\left[Z_{\mathrm{A}} \int \frac{\rho_{\mathrm{B}}(\bar{r})}{|R - \bar{r}_{\mathrm{A}}|}\, \mathrm{d}\bar{r} + Z_{\mathrm{B}} \int \frac{\rho_{\mathrm{A}}(\bar{r})}{|R - \bar{r}_{\mathrm{B}}|}\, \mathrm{d}\bar{r} \right] \tag{3}$$

where Z_i, R_i and ρ_i are the nuclear charge, the location and the electron density of the ith atom (i = A, B), in this case atom B being more electronegative than atom A. The latter is calculated from the empirical weighted Wolfsberg-Helmholtz formula,

$$H_{\mu\nu} = \tfrac{1}{2} K_{\mathrm{AB}} (H_{\mu\mu} + H_{\nu\nu}) S_{\mu\nu} \tag{4}$$

where μ and ν stand for the μth and the νth orbitals of atoms A and B, respectively.

Values of the diagonal elements for the Hamiltonian in equation (4) are experimentally based, and valence orbitals are given by the Slater form. K_{AB} and δ are adjustable empirical parameters in the range $1.4 \leqslant (1 + \kappa) \leqslant 2.5$ and $0 \leqslant \delta \leqslant 0.1$ nm. Then, K_{AB} is the K-parameter used for the EHMO method in the off-diagonal Hamiltonian matrix elements,

$$K_{\mathrm{AB}} = 1 + \kappa \exp[-\delta(R_{\mathrm{AB}} - r_0)] \tag{5}$$

where r_0 is the sum of atomic radii of atoms A and B. The diagonal Hamiltonian matrix elements are given by the $-$VSIP values taken from experimental and Hartree–Fock–Slater data. Slater's exponents are based on self-consistent calculations.

The following calculation procedure was employed to evaluate the interaction of a single H-atom with either the Pt(111) or Pt(100) single crystal surface in a simulated aqueous electrochemical environment, under an applied electric potential. The single H–Pt interaction is described by an adsorbed ensemble of the type $[\mathrm{Pt}_N \cdot H]$, where N is the number of Pt atoms of the high spin bilayer cluster used to model the Pt surface (Fig. 1). For Pt(111) and Pt(100) the values $N = 22$ and 25 were chosen, respectively. These figures represent the minimum values of N compatible with border effect-free calculations and constant binding energies. Clusters were geometrically built by keeping the Pt–Pt bond length constant at 0.277 nm. This figure agrees with the Pt–Pt interatomic distance in bulk Pt[32].

The H–Pt interaction energy is given by the specific VSIP value which defines the equilibrium potential of the system. This value is attained when the charge transfer at the equilibrium internuclear distance is close to that predicted from the electronegativity difference according to the Pauling's ionicity relationship[33]. Values of the initial parameters are assembled in Table 1, which was taken from[34].

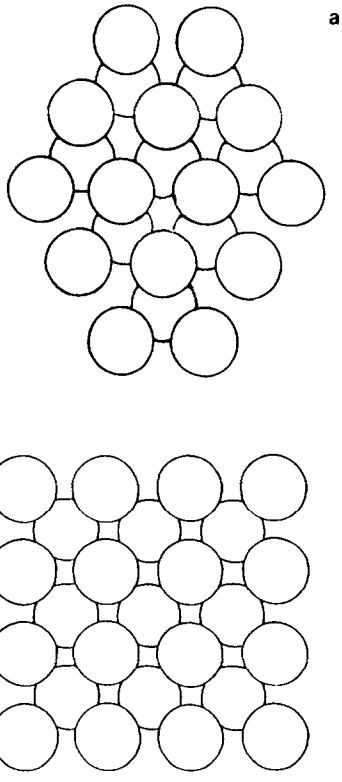

Fig. 1. Platinum cluster models. (a) $\mathrm{Pt}_{22}(111)$; (b) $\mathrm{Pt}_{25}(100)$. Complete and uncomplete circles indicate Pt atoms at the surface and subsurface layer, respectively.

Table 1. EHMO calculations: optimized parameters

Atomic orbital	VSIP(eV)	ζ_1(a.u.$^{-1}$)	ζ_2(a.u.$^{-1}$)	c_1	c_2
Pt 5d	−12.83	4.0950	1.8600	0.7980	0.3520
Pt 6s	−9.32	1.9830			
Pt 6p	−5.72	1.3440			
O 2s	−27.96	2.5640			
O 2p	−12.16	2.2640			
H 1s	−13.30	1.3000			

VSIP ≡ Valence state ionization potential.
$\zeta_{1,2}$ ≡ Exponents of the base generating functions.
$c_{1,2}$ ≡ Linear coefficients of the double zeta Pt *d*-orbitals.

Following the method previously described for Pt and H[35], VSIP and Slater orbital exponents were taken from[28]. Values $\delta = 0.035$ nm and $K_{AB} = 1.75$ have been set in equation (5) as those leading to the best description of both the bond length and the adsorption energy.

Positive applied electric potentials were simulated by shifting VSIP values from the Fermi energy level of Pt downwards[36, 37]. The influence of the applied electric potential on solvent adsorption was neglected. In a previous study[34], the change of VSIP with the applied electric potential was set equal to 1 as the simplest choice, because there was no experimental information that could justify a different dependence. On the other hand, for the H-atom electrosorption on Pt, it is reasonable to admit that the change in the geometry of the H-adsorbate ensemble with the applied electric potential is reflected by the characteristics of H-atom electrosorption voltammetric current peaks.

For a single H-adatom and a single water molecule interaction with the Pt single crystal surface, distinguishable adsorption sites, such as, on-top (one-fold), bridge (two-fold) and hollow (higher coordination) were considered. Adsorption at a hollow site implies a four-fold coordination on $Pt_{25}(100)$. Otherwise, either three or four Pt atoms can define the hollow H-atom or OH coordination on $Pt_{22}(111)$, depending on whether the fcc [(3–1)-hollow site] or the hcp [(3–3)-hollow site] local symmetry is involved, respectively. Obviously, several adsorption configurations are related to the interaction of either a single H-atom or OH-species with each one of those sites. In this work, different adsorption configurations and degrees of Pt surface coverage by H-atoms on both the top-most and underlying sites were systematically considered. In this case, the most stable OH-adsorbate configuration was chosen.

It should be noted that the similarities between theoretical calculations and real surface processes must be handled carefully because of the space limitation of finite clusters which can lead to different responses of the electronic distribution to a local interaction with small atoms. Unfortunately, it is difficult to extend *ab-initio* calculations, as those carried out for small ($N = 4$, 5) "testing" clusters[38], to large clusters ($N > 20$) built up with transition metals of high atomic numbers. In these cases EHMO calculations lead to results which can be compared with experimental data[27, 28, 34, 36, 37].

3. RESULTS

The formation of a stable H-adatom configuration implies that a minimum potential energy for the system is achieved. In the simulated aqueous electrochemical environment, calculations show that among all possible H-adatom configurations, those involving the bridge on Pt(100), and the hollow coordination together with neighbour H_2O or OH-adsorbates on Pt(111) are the most relevant. From spectroscopic data[23, 24] it was found that H-adatom bridge coordination for $Pt_{25}(100)$, and (3–1)-hollow coordination with neighbour on top OH-adsorbates for $Pt_{22}(111)$ are the most stable adsorbate configurations, in agreement with a full optimization in bond distance and planar angle for each adsorbate geometry (Fig. 2). The geometry and relative stability of each adsorbate can be inferred from data assembled in Table 2. Values of AE, the adsorption energy, were calculated from the difference:

$$AE = E_{T,Pt_NH} - E_{T,Pt_N} - E_H - E_{OH} \qquad (6)$$

where E_{T,Pt_NH} and E_{T,Pt_N} are the total energy for the $[Pt_N \cdot H]$ and the $[Pt_N]$ ensembles, respectively, E_H and E_{OH} stand for the energy term related to the free H-atom and OH-species, respectively.

The geometry optimization of adsorbed ensembles is obtained by changing simultaneously r_{Pt-H}, the Pt—H bond distance and the Pt—Pt—H planar

Table 2. Single atomic H adsorption energy, AE, optimized Pt–H distance, and perpendicular distance (h) from H-atom to the plane of the surface for $[Pt_{22}(111) \cdot H \cdot OH_2]$ and $[Pt_{25}(100) \cdot H]$ configurations at the equilibrium potential

$Pt_{22}(111)$	AE eV	r_{Pt-H} nm	h nm
on-top	0.0234	0.174	—
bridge	0.1239	0.180	0.104
hollow (3–3)	0.0786	0.175	0.020
hollow (3–1)	−0.8310	0.186	0.095
$Pt_{25}(100)$	AE eV	r_{Pt-H} nm	h nm
on-top	0.0126	0.176	—
bridge	−0.7831	0.187	0.112
hollow	0.0663	0.175	0.020

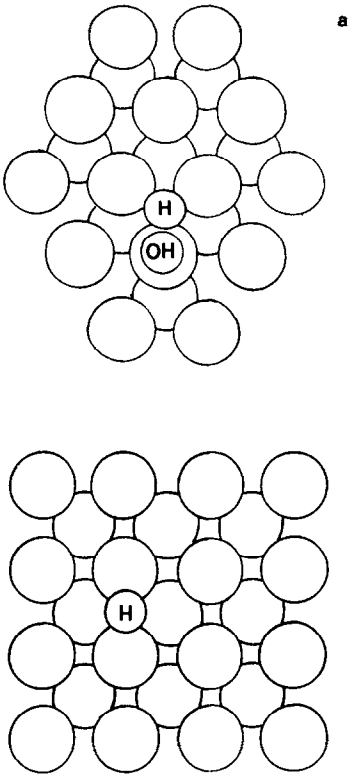

Fig. 2. H-atom structures involving surface Pt atoms at Pt clusters. (a) H-adatom (3–1)-hollow coordination and OH-adsorbate on-top coordination on $Pt_{22}(111)$. (b) H-adatom bridge coordination on $Pt_{25}(100)$.

angle. For this purpose, r_{Pt-H} was changed 0.001 nm stepwise from the initial $r_{Pt-H} = 0.160$ nm value up to a value at which the Pt—H bond rupture occurs. Correspondingly, for each r_{Pt-H} value the planar angle was fully optimized. The same geometry optimization was extended to the Pt—O—H bonds.

The adsorption bond resulting from the H—Pt interaction at the second Pt layer is similar to that previously calculated from a linear H—Pt coordination. No influence on the adsorption energy was found when larger Pt clusters were considered.

Data assembled in Table 2 show that the most stable structure of a single H-adatom on $Pt_{25}(100)$ corresponds to the bridge adsorbate geometry, whereas for a single H-adatom on $Pt_{22}(111)$ the largest adsorbate stabilization energy results for the (3–1)-hollow interaction with a neighbour on top OH-adsorbate ($r_{Pt-O} = 0.202$ nm, $r_{O-H} = 0.102$ nm). These results are rather different from those reported previously[37], since for the chosen parameters, OH-species are more likely to be adsorbed than a single water molecule.

The gradual Pt surface coverage by H-adatoms makes the adsorbate ensemble more stable on both $Pt_{25}(100)$ and $Pt_{22}(111)$ surfaces. It should be noted, however, that EHMO calculations made for water adsorption on $Pt_{25}(100)$ results in an unstable adsorbate for Pt fully covered by H-adatoms. These results are consistent with the H-adatom structures advanced over a decade ago for Pt from *in situ* infrared spectroscopy[22, 24].

The net charge variation in the H- and O-atom for the (3–1)-hollow adsorption with the applied electric potential was followed on $Pt_{22}(111)$. In this case, it was found that the O-atom charge strongly depends on the applied electric potential, since the O-atom is directly bonded to the Pt surface. On the other hand, the net charge on the H-atom bonded to the O-atom is almost constant in the range -1.0 to 1.0 eV, since the H-atom bound to the O-atom is located far from the Pt surface (Table 3). Likewise, no clear variation in the charge of the H-atom bonded to Pt with the applied electric potential could be observed (Table 3). These results indicate that the influence of the applied electric potential on the Pt surface is almost fully compensated by the more electronegative O-atom.

When the degree of surface coverage by H-adatoms increases, new stable H-adatom structures which are built at the centre of a four Pt atom cluster region, are found for both $Pt_{22}(111)$ and $Pt_{25}(100)$. The calculation of the stability of these structures is appropriate to describe possible H-adatom local interactions resulting from different degrees of Pt surface coverage. For the most stable H-adatom bridge configuration on $Pt_{25}(100)$ (Fig. 3), the stabilization of the adsorbed ensemble proceeds via a (2 × 2)-structure at a bridge coordination site, whereas for $Pt_{22}(111)$ (Fig. 4) the adsorbed ensemble energy is -0.13 eV, as would be expected for a physisorbed species. However, a H-adatom at a (3–1)-hollow site, together with an OH-adsorbate at an on-top neighbour site, gives a more realistic description of the H adsorbed ensemble.

Different local interactions and changes in the H-adatom adsorption energy on $Pt_{25}(100)$ are obtained at negative applied electric potentials. Likewise, the

Table 3. Charges on the O and H, q_O and q_H, of hollow $[Pt_{22}(111) \cdot H \cdot OH_2]$ ensembles at different applied electric potential (V)

V(eV)	1.0	0.5	0	−0.5	−1.0
q_O(ecu)	0.589	0.546	−0.501	−0.456	−0.406
q_{H_O}*(ecu)	0.404	0.405	0.408	0.408	0.408
q_H†(ecu)	−0.204	0.112	−0.073	−0.012	0.045

* Net charge on the H-atom bound to O-atom.
† Net charge on the H-atom bound to Pt.

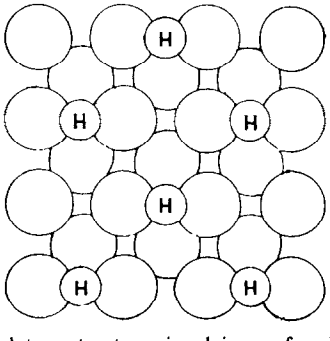

Fig. 3. H-adatom structures involving surface Pt atoms at Pt clusters. H-adatom bridge coordination on $Pt_{25}(100)$ for a degree of surface coverage ≅ 3/8.

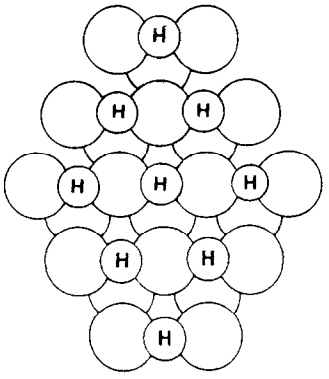

Fig. 4. H-adatom structures involving surface Pt atoms at Pt clusters. H-adatom bridge coordination on $Pt_{22}(111)$ for a degree of surface coverage $\cong 9/14$.

presence of a H-adatom at a hollow site directly bonded to a Pt-atom at the second layer, tends to shift the H-adatom from a bridge to an on-top site. Although the appearance of such complex geometry is rather unlikely (0.23 eV), it tends to become stable when the applied electric potential is below -0.1 eV. This type of H-adatom coordination involving both the first and second Pt atom layer for $Pt_{25}(100)$ is depicted in Fig. 5. Nevertheless, for applied electric potentials more negative than -0.35 eV, the stabilization of the H-adatom adsorbed ensemble decreases abruptly, and for -0.4 eV only physisorbed H-atom species are observed again on $Pt_{25}(100)$. For applied potentials even lower than -0.4 eV, negative net charges for H- and Pt-atoms are found. Correspondingly, a large repulsion energy between Pt and H atoms, which can not be compensated by the adsorption energy itself, appears.

A similar analysis was made for H-adatoms on $Pt_{22}(111)$. In this case, a H-adatom at a (3–1)-hollow site and an OH-adsorbate at a neighbour on-top site become the most likely adsorbate ensemble (Fig. 6), although values of AE correspond to physisorbed species when the applied electric potential is above -0.15 eV. On the other hand, for applied electric potentials below -0.35 eV, a further stabilization of the H-adatom interacting with a Pt atom at the second layer is observed. In this case, the corresponding AE value is free from the water coadsorption influence.

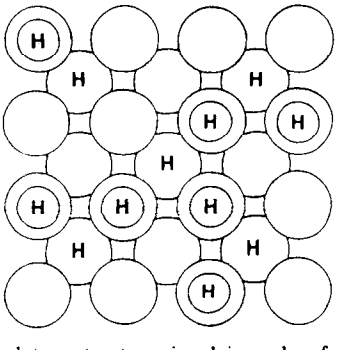

Fig. 5. H-adatom structures involving subsurface Pt atoms at Pt clusters. H-adatom on-top coordination on $Pt_{25}(100)$. Degree of surface coverage $\cong 7/16$; degree of suburface coverage $\cong 5/9$. H-atoms with and without a circle represent H-atoms interacting with either a surface Pt or a subsurface Pt atom, respectively.

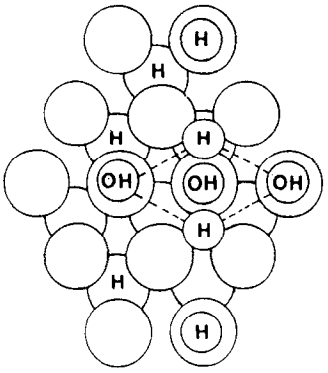

Fig. 6. H-adatom structures involving subsurface Pt atoms at Pt clusters. H-adatom bridge and on-top coordination on $Pt_{22}(111)$. Degree of surface coverage $\cong 2/7$; degree of surface coverage $\cong 3/8$. On-top coordinated neighbour OH-adsorbates are also shown.

For applied electric potentials below -0.5 eV the adsorbate ensemble is no longer stable, *ie* the AE changes from negative to positive. This change is due to a rather large net negative charge for both the H and Pt atom on $Pt_{22}(111)$.

The above description resulting from EHMO calculations implies the possible existence of several H-adatom states on Pt in the simulated aqueous electrochemical interface. In fact, the multiplicity of H-atom electrosorption voltammetric peaks has been associated with the formation of different H-adatoms on Pt in acid. The EHMO description also indicates that, under a high degree of surface coverage by H-atoms, H-adsorbates involving a Pt atom at the second layer would be also possible.

4. DISCUSSION

It is well known that H-atom electroadsorption on Pt results mainly in the formation of two different adsorbates, namely, the weakly and strongly adsorbed H-atom. For Pt(111) single crystal surfaces, the weak H–Pt bonding, in contrast to the strong H–Pt bonding for Pt(100), should involve the contribution of a water molecule to the formation of the adsorbed ensemble[37, 39–42], which can be formally represented as a $[Pt_N \cdot H \cdot OH_2]$ ensemble. *IR* spectroscopy data showed that the bond energy of weakly bound H-adatoms on Pt(111) depends on the applied electric potential (charge density)[13, 39]. Otherwise, strongly bound H-adatoms on Pt(100) imply an adsorbed ensemble in which the H-atom electron density is delocalized on the Pt surface[37].

Depending on whether the electron energy level is lower or higher than the Pt Fermi level, either negatively or positively charged H-adatoms result. This excess of charge results in a change in the shape of the potential energy curves, which in turn implies a change in both the H–Pt site interaction for each possible H-adatom coordination, and the polarization of molecules at the interface.

Our results show that the formation of H-adsorbates at surface Pt sites and subsurface Pt sites

in the simulated aqueous electrochemical environment becomes possible on both $Pt_{22}(111)$ and $Pt_{25}(100)$. Furthermore, results predict that a transition from surface to subsurface adsorbate configurations is feasible by adequately changing the applied electric potential. This finding provides a new insight into the nature of H-adatom species on Pt in both vacuum and aqueous environments. In fact, this type of configurational transition has been reported for Pd(111)[43], and the presence of subsurface H-adatom states at Pt, Pd and Ni single crystal electrodes as well[44, 45].

H-adatom subsurface states on Pt result from the H-adatom stabilization by an excess of negative surface charge which favours a transition from a H-adatom bridge coordination to a H-adatom hollow subsurface coordination on $Pt_{25}(100)$, and from a H-adatom (3–1)-hollow coordination to a H-adatom hollow subsurface coordination on $Pt_{22}(111)$ (Figs 5 and 6). H-adatoms bound to a surface Pt and a subsurface Pt atom are electronically different as a result of the excess of negative charge at the H-adatom bound to a subsurface Pt atom. These H-adatom subsurface states could probably be related to the Pt–H vibration frequency recorded near 0.05 V by electrochemically modulated infrared spectroscopy[22] and visible-infrared sum frequency generation vibrational spectroscopy[25].

On the other hand, the possible existence of H-adatoms at the subsurface level would introduce an additional state in those electrochemical processes in which H-atoms are involved. This can be visualized through the potential energy curves calculated from Morse equation[46] for the solvated proton (reactant) and the H-adatom bound to surface and subsurface Pt atoms (product) (Fig. 7). For this purpose, data assembled in Table 4 were used for the H-surface and H-subsurface adsorbates in the course of the H^+ ion discharge step.

The potential energy vs. either the r_{Pt-H} or r_{H-OH_2} distance (Fig. 7) plot represents the stabilization for the H_3O^+ ion in solution (curve 1), the H-adatom bound to a surface Pt atom (curve 2), and the H-adatom bound to a subsurface Pt atom (curve 3). The equilibrium Pt–H bond length is taken from the gas phase data, $r_{Pt-H} = 0.18$ nm[36]. The equilibrium distance in curve 1 is 0.22 nm, irrespective of the applied electric potential. For H-adatom formation on Pt two equilibrium distances are obtained, namely, 0.18 nm and 0.16 nm, depending on whether a Pt atom at the surface or at the subsurface is involved in adsorbate formation.

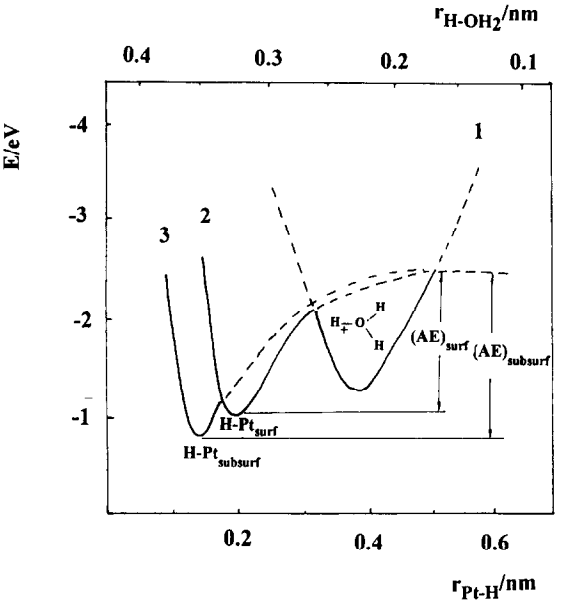

Fig. 7. Potential energy vs. r_{Pt-H} and r_{H-OH_2} diagram involving H^+-ion hydration (curve 1), H-adatom–surface Pt (curve 2) and H-adatom–subsurface Pt (curve 3) interactions. Calculations are based on data assembled in Table 4.)

The preceding description can be further improved by considering the change of the substrate lattice spacing with the applied potential, which is another problem of importance in dealing with electrochemically promoted H-absorption on metals[15].

5. CONCLUSIONS

- The EHMO quantum chemistry approach applied to the reversible H-atom electrosorption provides information about the possible existence of a H-adatom and OH-species bound to a surface Pt atom, and a H-adatom bound to a subsurface Pt atom.
- For $Pt_{22}(111)$ the stable H-adatom ensemble involving surface Pt comprises a (3–1)-hollow coordination and an on-top neighbour OH-adsorbate, whereas for $Pt_{25}(100)$ the stable H-adatom ensemble consists of a bridge coordination.
- For $Pt_{22}(111)$ the stable H-adatom ensemble involving subsurface Pt can be described as a (3–1)-hollow surface and (3–3)-hollow subsurface coordi-

Table 4. Parameters used in the calculation of the potential energy diagram shown in Fig. 7[46]

Morse equation, $E = E_{diss}\{1 - \exp[-a(r - r_0)]\}^2$
E = potential energy
E_{diss} = dissociation energy for either H–OH_2, H–Pt_{surf} or H–$Pt_{subsurf}$
$a = 0.18\,nm^{-1}$
Proton enthalpy of hydration = -269 kcal mol^{-1}
Hydrogen atom ionization energy = 313 kcal mol^{-1}
Pt work function (mean electron energy in the metal) = 120 kcal mol^{-1}
r_0(H–Pt_{surf}) = 0.18 nm
r_0(H–$Pt_{subsurf}$) = 0.16 nm

nation with OH-adsorbates as neighbours at on-top sites. Otherwise, for $Pt_{25}(100)$ the stable H-adatom ensemble implies a hollow subsurface and an on-top surface coordination, without OH-adsorbates.

- Morse potential energy curves for proton in solution, a H-adatom bound to a surface Pt atom, and a H-adatom bound to a subsurface Pt atom indicate that within the range 0 to -0.35 eV, the activation energy for the H^+ ion discharge reaction decreases because of the increase in the H-adatom subsurface Pt adsorption energy.

Acknowledgements—This work was financially supported by the Consejo Nacional de Investigaciones Científicas y Técnicas (Argentina). C. F. Z. is a member of the Programa de Desarrollo de Ciencias Básicas (Uruguay).

REFERENCES

1. A. Frumkin, in *Advances in Electrochemistry and Electrochemical Engineering* (Edited by P. Delahay and C. W. Tobias) Vol. 3, Interscience, New York (1963).
2. R. Parsons, *Trans. Faraday Soc.* **54,** 1053 (1958).
3. H. Gerisher, *Z. Phys. Chem.* **8,** 137 (1956).
4. B. E. Conway and J. O'M. Bockris, *J. Chem. Phys.* **26,** 532 (1957).
5. J. Horiuti and M. Polanyi, *Acta Physicochim. U.R.S.S.* **2,** 505 (1935).
6. J. O'M. Bockris, in *Modern Aspects of Electrochemistry* (Edited by J. O'M. Bockris) Vol. 1, Chap. 4, Butterworths, London (1954).
7. B. E. Conway and L. Bai, *Electrochim. Acta* **31,** 1013 (1986).
8. B. V. Tilak and B. E. Conway, *Electrochim. Acta* **21,** 745 (1976).
9. B. V. Tilak, C. G. Rader and B. E. Conway, *Electrochim. Acta* **22,** 1167 (1977).
10. A. T. Hubbard, R. M. Ishikawa and J. Katekaru, *J. electroanal. Chem.* **86,** 289 (1978).
11. N. Markovic, N. Marinkovic and R. Adzic, *J. electroanal. Chem.* **241,** 309 (1988).
12. J. Clavilier, K. El Achi and A. Rodes, *Chem. Phys.* **141,** 1 (1990).
13. F. T. Wagner and T. E. Moylan, *Surf. Sci.* **182,** 125 (1987).
14. K. Bange, D. Grider and J. K. Sass, *Surf. Sci.* **126,** 437 (1983).
15. I. M. Tidswell, N. M. Markovic and P. N. Ross, *Phys. Rev. Lett.* **71,** 1601 (1993).
16. D. A. Harrington and B. E. Conway, *J. electroanal. Chem.* **221,** 1 (1987).
17. L. Gao and B. E. Conway, *Electrochim. Acta* **39,** 1681 (1994).
18. R. M. Torresi, O. R. Camara, C. P. de Pauli and M. C. Giordano, *Electrochim. Acta* **32,** 1301 (1987).
19. T. Frenlink, W. Visscher and J. A. R. van Veen, *Electrochim. Acta* **40,** 545 (1995).
20. H. Gerischer and W. Mehl, *Z. Elektrochem.* **59,** 1049 (1955).
21. M. W. Breiter, H. Kammermaier and C. A. Knorr, *Z. Elektrochem.* **60,** 37 (1956).
22. R. J. Nichols and A. Bewick, *J. electroanal. Chem.* **202,** 101 (1986).
23. A. Bewick, K. Kunimatsu, J. Robinson and J. W. Russell, *J. electroanal. Chem.* **132,** 175 (1981).
24. A. Bewick and J. W. Russell, *J. electroanal. Chem.* **132,** 329 (1982).
25. A. Tadjeddine and A. Peremans, Abst. from *Surface Science and Electrochemistry* IUVSTA '94, p. 40 (L 24), San Benedetto del Tronto, 12–16 September (1994), Italy.
26. R. Hoffmann, *J. Phys. Chem.* **39,** 1797 (1963).
27. A. B. Anderson and R. Hoffmann, *J. Phys. Chem.* **60,** 4271 (1974).
28. A. B. Anderson, *J. Phys. Chem.* **62,** 1187 (1975).
29. G. Calzaferri, L. Forss and I. Kamber, *J. Phys. Chem.* **93,** 5366 (1989).
30. G. Calzaferri and R. Hoffmann, *J. Chem. Soc. Dalton Trans.* 917 (1991).
31. M. Brändle and G. Calzaferri, *Helvetica Chimica Acta* **76,** 924 (1993).
32. D. R. Lide, Ed. *CRC Handbook of Chemistry and Physics*, CRC Press, Boca Raton, FL, 1990–91.
33. L. Pauling, *The Nature of the Chemical Bond*, 3rd edn., Cornell University Press, Ithaca, New York, p. 45 (1992).
34. C. F. Zinola, G. L. Estiú, E. A. Castro and A. J. Arvia, *J. Phys. Chem.* **98,** 1766 (1994).
35. G. Calzaferri and M. Brändle, *QCMP 116*, QCPE Bulletin, Vol. 12, No. 4 (1992).
36. G. L. Estiú, S. A. Maluendes, E. A. Castro and A. J. Arvia, *J. electroanal. Chem.* **284,** 289 (1990).
37. G. L. Estiú, S. A. Maluendes, E. A. Castro and A. J. Arvia, *J. Phys. Chem.* **92,** 2512 (1988).
38. K. Przybylski, J. Koutecky, V. Bonacic-Koutecky, P. von Ragué-Schleyer and M. F. Guest, *J. Chem. Phys.* **94,** 5533 (1991).
39. J. P. Candy, P. Fouilloux and M. Primet, *Surf. Sci.* **72,** 167 (1978).
40. A. M. Baró, H. Ibach and H. D. Bruchmann, *Surf. Sci.* **88,** 384 (1979).
41. F. T. Wagner and P. N. Ross Jr. *Surf. Sci.* **160,** 305 (1985).
42. J. O'M. Bockris and D. B. Matthews, *Proc. Roy. Soc.* **A292,** 479 (1966).
43. T. E. Felter, E. C. Sowa and M. A. Van Hove, *Phys. Rev.* **B40,** 891 (1989).
44. A. Wieckowski, *J. Chim. Phys.* **88,** 1247 (1991).
45. J. Rogan, M. Lagos and I. K. Schuller, *Surf. Sci.* **318,** L1165 (1994).
46. E. A. Moelwyn-Hughes, *Physical Chemistry*, 2nd Edn, Ch. 10, Pergamon Press, Oxford (1961).